Surface charge and interactions of 20-nm nanocolloids in a nematic liquid crystal

A. V. Ryzhkova,[1,3] M. Škarabot,[1] and I. Muševič[1,2]

[1]*Condensed Matter Physics Department, Jožef Stefan Institute, Jamova 39, SI-1000 Ljubljana, Slovenia*

[2]*Faculty of Mathematics and Physics, University of Ljubljana, Jadranska 19, SI-1000 Ljubljana, Slovenia*

[3]*Electrical Engineering Technologies Laboratory, Department of Physics, South Ural State University, Lenina ave.76, 454080 Chelyabinsk, Russia*

(Received 28 January 2015; published 17 April 2015)

We studied real-time motion of individual 20-nm silica nanoparticles in a thin layer of a nematic liquid crystal using a dark-field optical videomicroscopy. By tracking the positions of individual nanoparticles we observed that particle pair interactions are not only mediated by strong thermal fluctuations of the nematic liquid crystal, but also with a repulsive force of electric origin. We determined the total electric charge of silanated silica particles in the nematic liquid crystal 5CB by observing the electric-force-driven drift. Surprisingly, the surface electric charge density depends on colloidal size and is $\sim 4.5 \times 10^{-3}$ C/m^2 for 20-nm nanocolloids, and two orders of magnitude lower, i.e., $\sim 2.3 \times 10^{-5}$ C/m^2, for 1-μm colloids. We conclude that electrostatic repulsion between like-charged particles prevents the formation of permanent colloidal assemblies of nanometer size. We also observed strong attraction of 20-nm silica nanoparticles to confining polyimide surfaces and larger clusters, which gradually results in complete expulsion of nanoparticles from the nematic liquid crystal to the surfaces of the confining cell.

DOI: 10.1103/PhysRevE.91.042505 PACS number(s): 61.30.−v, 47.57.J−, 64.75.Yz, 68.60.Dv

I. INTRODUCTION

There is a permanent and broad interest in particle dispersions, because of their high potential for both fundamental studies and practical applications, such as display devices [1,2], drug carriers [3], laboratory-on-a-chip devices [4], and as a precursor for various advanced materials, including the colloidal crystals for photonic applications [5–8]. Recently, there has been a growing interest in studies of nanoparticle (NP) dispersions due to their ability to tune and tailor the physical properties of host materials [9–11].

Mixtures of nanoparticles and liquid crystals are a new type of composite materials with tunable electric, optical, and elastic properties. For example, the spatial distribution of nanoparticles enables the control of microscopic performance of the material [12–16]. Nanocolloids are actively used for stabilization of the blue and twist grain boundary (TGB) phases [17,18]. In this case, spherical gold nanoparticles with mean diameter of several nanometers expand the temperature range of cholesteric blue phase for an order of magnitude, while the clearing temperature is only moderately decreased [17]. Nematic dispersions of gold nanorods promise a new approach to modulate the polarized scattering intensities of individual gold nanorods by using liquid crystals with low driving voltages [19]. Extension of this method could give us a possibility to actively control optical antennas as well as other plasmonic elements. Liquid crystal dispersions of quantum dots of nanometer size are promising fluorescent material that could be used as a light source in liquid crystal display applications. Nanocolloids are also actively used for solar cell applications. For instance, in hybrid solar cell, consisting of a polymer, a discotic liquid crystal, and ZnO nanoparticles, discotic liquid crystal ligands improve the compatibility between P3HT polymer and ZnO nanoparticles, which is beneficial for enhanced charge separation and transfer efficiency [20].

In all described systems the thermodynamic stability of the nanocolloidal dispersion plays an important role. Surprisingly, there are relatively few publications analyzing the stabilization processes of nanocolloidal dispersions in liquid crystals [21]. It is generally believed that stabilization of nanoparticles dispersion in liquid crystals is difficult and always results in agglomeration or/and phase separation because of the long-range elastic attraction between colloidal inclusions [22,23]. Namely, in the NLC, the long-range pair attraction appears due to the elastic distortions created by the alignment of the NLC molecules on the surfaces of inclusions. The total free energy of a colloidal pair depends on the separation between the two particles. Therefore, the particles always attempt to minimize it by assembling in different aggregates [24–34]. Contrary to the theoretical predictions [23], the long-range colloidal attraction in the NLC was recently observed also for nanocolloids with the diameter as small as ∼30 nm [35]. The strength of attraction and permanent binding fades with decreasing particle's size and other mechanisms start to play an important role for particle sizes below 20 nm.

In our recent work [35], we presented a systematic study of colloidal pair interaction in the NLC by using a series of silica microspheres with equal chemical constitution and surface treatment with variable sizes from micrometers down to 22 nm. In that work we noticed that permanent binding of a colloidal pair could be obtained in the NLC for nanoparticles as small as 30 nm, but below that size, Brownian motion prevented the formation of stable colloidal pairs. The reasons for this remained unclear.

Here we show that the reason for observed instability of pairs of 20-nm particles in the NLC is the electric repulsive force between like-charged surfaces of silica particles and strong Brownian motion of nanoparticles that prevents permanent binding. The presence of surface charge is clearly demonstrated in electrokinetic experiments, where colloidal nanoparticles are driven in motion by an external electric field. We found that the surface charge density depends on the size of the colloidal particle, and is proportional to $1/d$, where d is the

particle diameter. A competition between the elastic-attractive and electric, repulsive colloidal forces leads to the formation of metastable nanocolloidal pairs, which exist within a few minutes and than dissociate into two individual particles. Moreover, we show that nematic dispersion of nanoparticles is strongly affected by the two confining polyimide surfaces of the measuring cell. These surfaces are very strong attractors for silanized silica nanoparticles, which are in the course of time expelled from the NLC and accumulate on the surfaces.

II. MATERIALS AND METHODS

The experiments have been carried out with fluorescently labeled silica nanoparticles with diameter 20 nm, 35 nm, 60 nm, and 90 nm (Micromod). The particles contain a high amount of covalently bound rhodamine B ($\lambda_{ex} = 569$ nm; $\lambda_{em} = 585$ nm) and are extremely stable in organic solvents and buffers. In this work we did not use the fluorescence microscopy to track the positions of the particles; these particles were used merely to have comparable results to our previously published work [35] on the same type of particles, but with larger sizes. Strong homeotropic surface anchoring of the nematic LC molecules was ensured by functionalizing the particles with N,N-dimethyl-n-octadecyl-3-aminopropyl-trimethoxysilyl chloride (DMOAP). The particles were dispersed in 2% DMOAP-water solution and mixed for 5 min. DMOAP chemically bonded to the particles' surfaces forming a well-defined monolayer. After mixing and stirring, the particles were washed with distilled water several times in order to remove excess DMOAP, and dried for 1 h at 120 °C. The particles were then dispersed in 5CB liquid crystal (4-pentyl-4-cyanobiphenyl) at a concentration around 100 ppm. After dispersing, we found that the nanoparticles formed aggregates in 5CB, which most likely formed during the drying procedure. Breaking these aggregates was accomplished by sonificating the dispersion with a powerful ultrasonic laboratory homogenizer (UP200St) positioned in the water bath with the sample. The sonification time had to be increased with the decrease of particle diameter and was as long as 1 h for 20-nm colloids. As prepared, the dispersions were stable for 12–24 h. Pair interactions of nanocolloids were studied in planar aligned glass cells (Brewer Science, polyimide PI 5291) with a variable gap between 2.5 μm and 6 μm that was filled with the 5CB-colloidal dispersion.

We have used the dark-field microscopy (DF) as a method to observe and trace the time-dependent position of nanocolloids in 5CB. This method is a powerful tool to characterize the nanocolloidal dynamics in LCs [36], and can be also used with dielectric nanoparticles [37]. The optical microscope Nikon Eclipse was equipped with special oil immersion dark-field condenser (Nikon, NA 1.43-1.20) for high contrast dark-field imaging. This condenser permits one to operate with immersion and high magnification objectives and was crucial for imaging and tracking of nanocolloids. The rays of light from the light source travel in a hollow cone formed by the condenser, pass through the objective, and illuminate the the object at its focal point at very large angles. In this way, the imaging objective collects only the light, which is scattered from the illuminated particle in forward direction and there is no background light. This enables us to take images of even the smallest nanocolloids (i.e., 20 nm) with a rather high optical contrast, because of a very dark background. To determine the trajectories of nanoparticles, their motion was recorded by a high speed ultrasensitive camera (Neo CMOS, Andor Inc.). Rather small pixel size of 6.5 μm of this camera assisted in a very good spatial resolution of our videotracking system. The single-particle position as a function of time was determined from the sequence of recorded images by using particle tracking software with an accuracy of $\pm$50 nm. Single colloids in the sample were distinguished from other inclusions and colloidal clusters by observing the Brownian motion and monitoring the scattered light from the particles. The diffusivity of colloidal agglomerates is much smaller compared to a single nanoparticle and they appear less mobile. We also observed that the shape and brightness of the clusters of particles is much different than a single colloidal nanoparticle, which is less bright and has a circular shape.

To manipulate a single nanocolloid, the laser tweezers setup based on acousto-optic deflectors, controlled by computer system and the IR laser, was used (Aresis, Tweez, $\lambda =$ 1064 nm). In this case the nanoparticles migrate due to thermally induced gradient of the order parameter, obtained by locally focused IR laser, which locally heats the nematic LC. These inhomogeneities of the order parameter are very efficient trapping sites for micrometer colloids, nanometer-size fluorescent molecules, and nanoparticles dispersed in the nematic LC [38].

The electrokinetic experiments were performed for the particle surface charge measurements. In order to observe the electrophoretic motion of nanocolloids directly, the obtained NLC dispersion was introduced in a specially designed liquid crystal cell. The cell consisted of two glass substrates separated by the Mylar spacers. On the lower substrate two in-plane ITO electrodes were formed using a photolithography method. The length of the electrodes was 20 mm and the width was 2 mm. The electrodes were separated by $d_0 = 100$ μm. The upper substrate was made of a bare glass with thickness of 150 μm. The cell thickness was set to 10 μm. Both glass substrates were covered by polyimide (PI 5291) and unidirectionally rubbed (parallel to the long side of an electrode, $\perp E$) in order to provide a planar alignment of the cell. The electrodes were connected to a generator (HMF2525, Hameg Instruments), oscilloscope (HM303-6, Hameg Instruments), and a high-voltage amplifier (A400, FLC Electronics). The nanoparticle dynamics was studied using the dark-field microscopy technique with videotracking of recorded images.

III. RESULTS AND DISCUSSION

A. Pair interaction of 20-nm nanoparticles in the nematic LC

It has been previously shown that nanoparticles in the range of 35–90 nm are capable of forming permanently stable pairs [35]. However, the stable pair is not the only formation, which appears in the nematic liquid crystal. A detailed analysis of a larger number of 20–90 nm pairs showed that other forms are present as well. One can roughly divide them into three categories: stable pairs, metastable pairs, and pairs without measurable interaction (no pairs).

The different particle behavior can be resolved by monitoring the time dependence of the trajectories of particles. In Fig. 1 one can see three different behaviors of colloidal pairs, which resulted in the formation of a stable pair [(a),(b)], a metastable pair [(c),(d)], or no-pair [(e),(f)]. On the plots, the black lines represent the time dependence of the separation r between two particles. The blue and red lines are the separations of the first and the second colloidal particle from their initial positions as a function of time. The analysis of these curves gives clear understanding of the processes, which take place during the interaction time. For instance, in the set of consequent images in Fig. 1(a), one can clearly see that after the two 35-nm particles were initially separated by about 3.5 μm, the separation between the particles gradually reduces with time, and after nearly 50 s it vanishes and the particles form a stable pair for a long time. We show in Figs. 1(a) and 1(b) the interaction of 35-nm-diameter colloids as an example, since no stable pair was found for smaller particles, such as the 20-nm colloids.

In the set of images in Fig. 1(c), one can clearly see that, after ~60 s, the two 20-nm colloidal particles form a bound pair, which is, however, unstable. At ~80 s, the pair is dissociated again, and it associates again at ~110 s. This clearly indicates the formation of a meta-stable pair of 20-nm colloidal nanoparticles, with a binding energy close to the thermal energy, available to the nanoparticle.

Figure 1(d) shows the corresponding positions of both particles and their separation, which over all period of time of interaction remains below 2 μm, although the distances between the particles and their start positions r_1, r_2 increase up to 8–10 μm. These trajectories therefore describe a randomly moving, weakly interacting pair (a metastable pair), which migrates far away from its starting point. It is important to mention that a metastable pair exists as a pair only for a certain period of time, usually, from 40 to 100 s. After that, it dissociates into two individual particles.

The third possibility is shown in the set of images in Fig. 1(e), and the corresponding separations are shown in Fig. 1(f). Here, the separation between the two 20-nm particles increases monotonically with time. In 90 s, the colloidal particles are separated by 8 μm and around 4 μm away from their initial positions. No pair is therefore formed at any time of observation.

More than 30 experiments with 20-nm particles were analyzed using dark-field microscopy. The observation time for each experiment started when two colloids were separated by ~2 μm, and finished when the separation between the particles exceeded ~8 μm. More than half of the experiments with 20-nm particles showed a metastable pair behavior, shown in Figs. 1(c) and 1(d). In the rest of experiments, the particles showed no measurable attraction, similar to a pair, shown in Figs. 1(e) and 1(f). We have not observed any permanent binding of two 20-nm single colloidal particles in more than 30 experiments performed.

In Fig. 2 one can see the distribution ratio of stable pairs, metastable pairs, and pairs of colloidal silica particles, which experienced no measurable attraction, as a function of the particle size. One can clearly see that the number of stable pairs drastically reduces by decreasing the particle's size. For 20-nm particles, no stable pairs are ever observed, though, statistically, the particles still experience some attractive interaction and build up metastable pairs, which live within several minutes and then dissociate into two individual colloids. The other commonly observed form of existence are individual, noninteracting particles, which appear in the vicinity of each other, but experience no measurable interaction.

These three categories are determined by the strength of the elastic pair interaction between the colloids. The elastic interaction is due to the elastic distortions of the nematic liquid crystal, caused by a suspended inclusion, which forces one to align the surrounding nematic liquid crystal on its surface. It was shown previously that these distortions can greatly exceed the particle size and are determined by the functional groups, which are attached to the particle's surface. In our case this is the DMOAP, chemically bound to the silica surface. For small particles, the surface area is substantially lower than for the big ones.

Currently, there is no evidence that the functional groups are distributed evenly over all silica nano-particle's surface and their quantity is similar for each colloid. Moreover, the atomic force microscope studies of a NLC-DMOAP interface by Kočevar and Muševič [39] demonstrated substantial inhomogeneities of the DMOAP monolayer coverage density on glass, where submicrometer voids were observed in *in situ* imaging of the NLC-DMOAP interface. Most likely, this kind of surface coverage inhomogeneities are also present in our silica nanoparticles, which can result in a difference in attraction force between two small particles. For instance, about half of 20-nm particles experience no interaction and the rest of the particles form metastable pairs.

The analysis of cross-correlation function of two colloids shows that the interparticle interaction potential for a metastable pair is below $\sim 10 k_B T$. This estimation can be considered just as an approximation, and there are two possible reasons for that: a broad variation of the surface anchoring of the colloids and a calculation error. The calculation error comes from the fact that we can do the measurement of the colloid position with a certain precision. The reason for finite precision may be in the overlapping of two particle's images as well as neglecting the three-dimensional nature of the particles' motion, which leads to erroneous estimation of colloidal positions [40]. Since the attraction potential for 20-nm particles is very shallow, we cannot exclude the influence of the other interaction forces, such as the van der Waals attraction or like-charge attraction [41], which possibly could influence the particle's dynamics. The origin and impact of these effects shall remain debatable.

B. Surface charge of 20-nm particles in the NLC

Our observations clearly show that 20-nm colloids in several cases attract each other, but they do not form stable pairs or assemblies in any of the 30 experiments that were performed. The question therefore is which force is responsible for this weak binding: is it only rather weak elastic attraction that cannot withstand strong Brownian motion, or is there another repulsive force, which becomes important for such small diameters of the nanoparticles in the NLC? Here, we show that the silanated silica nanoparticles in the 5CB NLC are electrically charged, which causes the electrostatic repulsion and prevents the formation of stable 20-nm colloidal pairs.

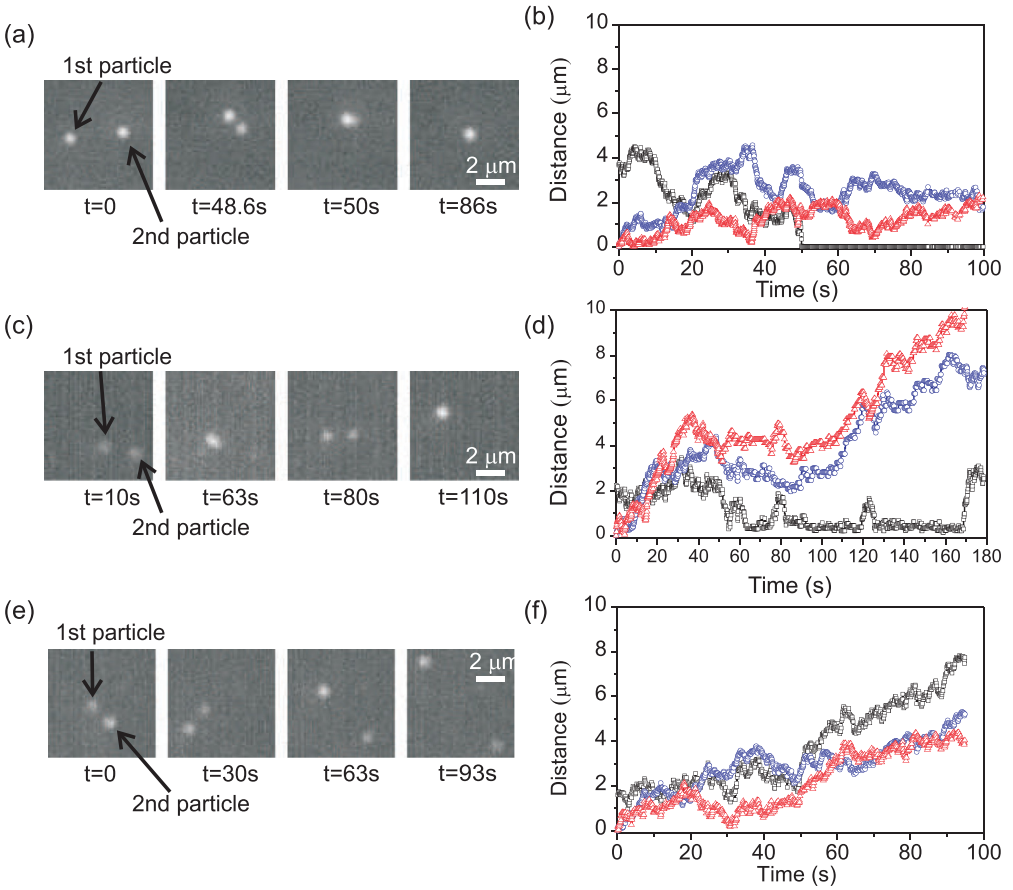

FIG. 1. (Color online) Snapshots of pair interaction and the trajectories of two colloidal particles, initially situated at a separation of 2–3 μm. (a) Two 35-nm diameter silanated silica particles form a stable pair within one minute of interaction. (b) Blue circles and red triangles denote the separation of each particle from its origin. Black squares denote the time dependence of the separation between the two particles. (c) Set of consecutive images of interacting 20-nm particles, which form a metastable pair. (d) The corresponding separations of each particle from the origin (blue circles and red triangles); black squares are the time dependence of the separation between the two particles. Note little "bumps" in the separation at 80 s and 120 s, which show temporal dissociation of the pair. (e),(f) Two 20-nm diameter particles experience no interaction. Black squares show the distance between two particles. Blue circles and red triangles correspond to the separation of the first and second colloid from the initial position.

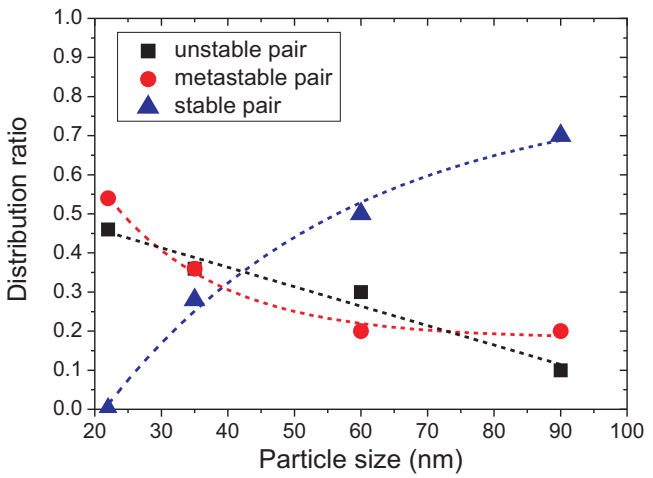

FIG. 2. (Color online) Distribution ratio of finding a stable pair, a metastable pair, and pairs of noninteracting particles, as a function of the diameter of the silanated silica nanoparticle in a planar 5CB. The lines are guides to the eyes only.

The electric properties of DMOAP-NLC interfaces were investigated some time ago using the AFM force spectroscopy [42,43]. It was clearly demonstrated that the DMOAP silanated glass surface is electrically negatively charged when in contact with a nematic LC, such as 5CB or 8CB in the isotropic phase. The surface charge densities for large and flat glass substrates were typically of the order of $\sim 10^{-4}$ C/m^2, whereas the Debye's screening lengths were of the order of $\sim$70–100 nm [42,43]. The surface electric charge plays no role in the pair interaction of relatively large microparticles in the NLCs, because the surface-to-surface separation of colloidal particles is typically $\sim\mu$m, and is much larger than the Debye screening length, λ_D. However, when the colloidal diameter is decreased and becomes comparable to λ_D, then in a close vicinity, the particles' electrically screened ionic layers start overlapping and colloids with the same electric charge start repelling each other.

The thickness of the Debye screening layer for a plane is given by $\lambda_D = \sqrt{\varepsilon_{\rm LC}\varepsilon_0 k_B T/(8\pi n_{\rm ions} z^2 e^2)}$. Here $\varepsilon_{\rm LC} = \varepsilon_{\parallel} =$ 20.3 due to the homeotropic anchoring of NLC molecules

on the particle's surface, ε_0 is the vacuum permittivity, k_B is the Boltzmann constant, $T = 298$ K is the temperature, $z = 1$ is the valence, $e = 1.6 \times 10^{-19}$ C is the elementary charge, and n_{ion} is the ion concentration. Here, the n_{ion} can be calculated via the expression [16] $n_{\text{ions}} = d_{\text{LC}}/(ze\mu R_{\text{LC}}S)$, where $d_{\text{LC}} = 6.3 \times 10^{-6}$ m is the thickness of the NLC cell, $\mu \sim 2 \times 10^{-10}$ m^2/V $\times$ s ($T = 296$ K) is the ion mobility at the given temperature [44], S $= 10^{-4}$ m^2 is the surface of the active NLC cell area, and $R_{\text{LC}} = 10^7$ Ω is the resistivity. Hence $n_{\text{ions}} \approx 2 \times 10^{20}$ m^{-3} and $\lambda_D \approx 76$ nm in our experiments. The obtained value is in a good agreement with the measurements of the Debye screening length ~55 nm of the silinated glass substrate performed with AFM (atomic force microscopy [43]. Unfortunately, from our optical experiments it is very difficult to estimate the exact distance at which the particles start to repel. First, in addition to the repulsion force, the nanoparticles are subjected to high thermal fluctuations in all three dimensions. This leads to the erroneous conclusions concerning the estimation of the center-to-center distance between two nanocolloids. Second, when the two particles approach each other, their images start to overlap and, therefore, it is not possible to accurately trace the single colloid's position anymore.

We determined the number of elementary charges on the nanoparticle's surface by using the Stokes drag method, where the particle's dynamics is studied in a cell with in-plane electrodes. The colloids are positioned in the center of the gap between the electrodes, and then the electric field is applied [45]. In the presence of an external ac electric field, the particle starts oscillating, as shown in Fig. 3(a). The oscillation amplitude of the nanoparticle is about ± 1.5 μm. The applied electric-field frequency is 1 Hz, the electric-field strength is 10^5 V/m, and the waveform is rectangular. The particle motion is recorded at a rate of 25 frames per s, and the particle position is determined at a given time by particle tracking software.

Figure 3(b) shows the velocity of the particle as a function of time. The experimental results are well fitted with a rectangular signal, where the electric-field strength (E) is varied in the range from 0.1×10^5 to 2.4×10^5 V/m. The E range is chosen so to avoid the influence of the nonlinear regime [46–49] that might appear at high electric fields, as well as any possible reorientation of the NLC [45]. The average colloid's velocity is derived from the measured displacement. Figure 3(c) clearly shows the linear dependence of the average particle velocity on the applied electric-field strength.

Using the force balance equation, $qE = 6\pi\eta r v$, one can estimate the particle's charge $q = 6\pi\eta r v/E$. From the Stokes-Einstein relation, it follows that $6\pi\eta r = k_B T/D$, where D is the self-diffusion coefficient of the nanoparticle. For ~20-nm colloids, D is approximately 4.65×10^{14} m^2/s, at $T = 298$ K [35].

Figure 4(a) shows the measured total electric charge on the nanoparticle as a function of the diameter of the particle. Surprisingly, the total amount of the electric charge is not proportional to the square of the particle's diameter, as expected for size-independent surface charge density, but follows a more moderate increase at larger diameters. This means that the surface charge density is higher for smaller particles and the corresponding electric field is also higher for smaller particles, therefore enhancing the alignment of NLC molecules perpendicular to the surface of the particles. This is shown in Fig. 4(b), where the surface charge density, determined from the experimental data points in Fig. 4(a), is proportional to the inverse diameter of the particle.

One can see from Fig. 4(a) that the total charge of a 20-nm particle is approximately $z \sim 35$ electron charges, which corresponds to a surface charge density $\sigma \sim 4.5 \times 10^{-3}$ C/m^2. This is two orders of magnitude larger surface charge density compared to the charge densities of $\sigma \sim$ (6–10) $\times 10^{-5}$ C/m^2, determined by the AFM force spectroscopy on flat silanated glass [42]. Thus the electric field at the particle's surface [50] is $\sigma/(\varepsilon_{\parallel} \cdot \varepsilon_0) \sim 25$ V/μm. We should stress that this value of the electric field at the surface of nanocolloids depends

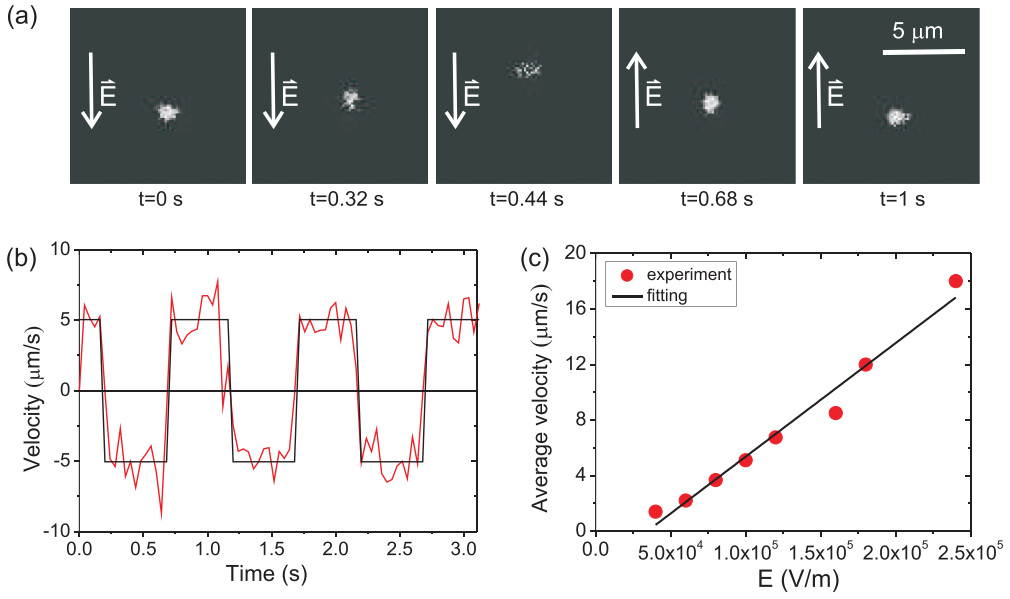

FIG. 3. (Color online) (a) Dark-field images of 20-nm DMOAP-coated silica particles moving along the applied electric field. (b) Time dependence of the particle velocity. The parameters of the applied electric field are the following: the electric-field strength is 10^5 V/m, the wave form is rectangular, and the frequency is 1 Hz. (c) The dependence of the average particle's velocity on the applied electric-field strength.

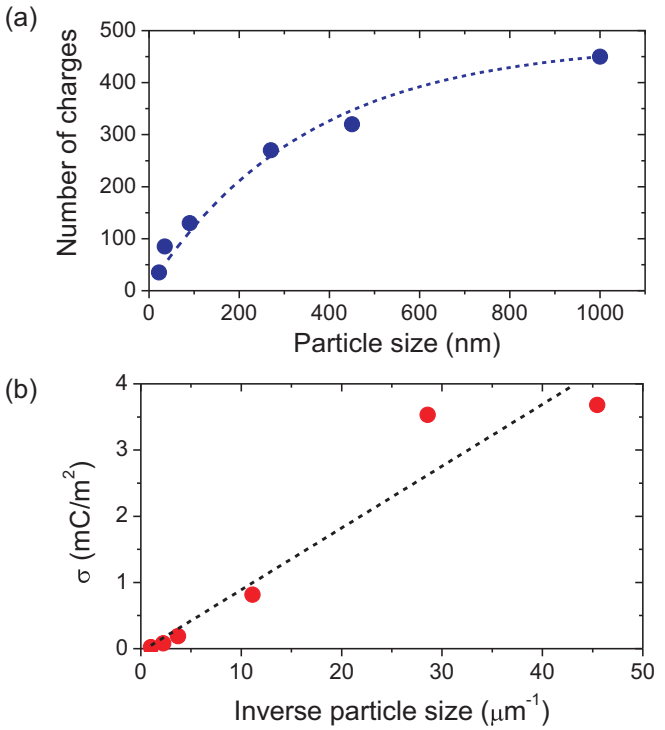

FIG. 4. (Color online) (a) Total electric charge of DMOAP silanated silica nanoparticle as a function of its diameter. Dotted line is a guide to the eyes only. (b) Surface charge density of a particle, determined from data in panel (a), as a function of inverse diameter of the particle. The dotted line is the best linear fit.

strongly on the diameter of the surface, where the charges are located. The field might be strong enough to influence the NLC director field close to and in the vicinity of the surface of a nanocolloid. Therefore, for positive dielectric anisotropy of a LC, the total surface anchoring will be sufficiently larger than the theoretical predictions, which takes into account just anchoring established by the DMOAP surfactant.

On the other hand, the surface charge density is much lower for larger diameter particles. For example, the total charge of an ∼1000-nm particle is approximately $z \sim 450$ electron charges, which corresponds to a surface charge density $\sigma \sim 2.3 \times 10^{-5}$ C/m^2. Surprisingly, this value is very close to the surface charge densities of $\sigma \sim (6–10) \times 10^{-5}$ C/m^2, determined by the AFM force spectroscopy on flat silanated glass [42]. In those experiments, the surface charge is determined from the measured electric force between a flat silanated glass surface and a micrometer sphere, mounted on an AFM cantilever. This is an interesting result, pointing to the fact that surface charge density is enhanced for larger curvature interfaces, and plays an important role for nanometer diameter particles in the nematic LCs.

C. Surface trapping and cluster attraction of 20-nm nanocolloids

Our observations show that prepared NLC dispersion of 20-nm DMOAP silanized silica nanoparticles remains homogeneous within about 24 h in a bulk sample. Moreover, we saw

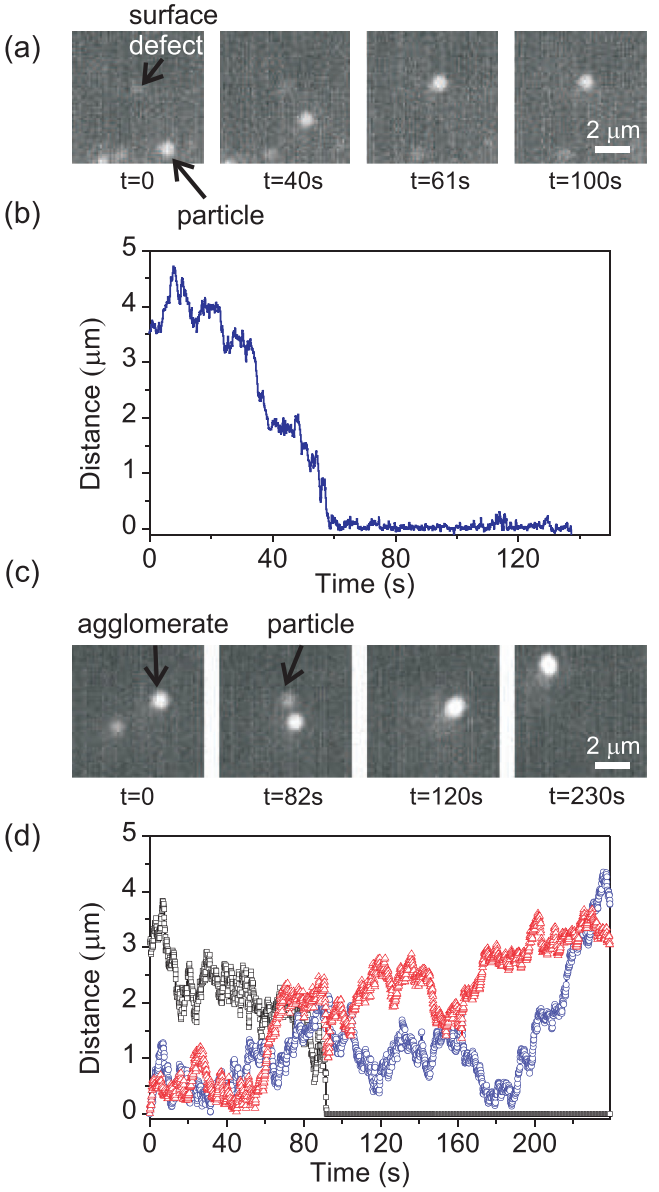

FIG. 5. (Color online) (a) Dark-field images of a 20-nm silica colloid, approaching a surface defect. (b) The corresponding distance between the 20-nm particle and the surface defect. (c) Dark-field images of a single 20-nm colloid, being trapped by a larger cluster of nanoparticles. Note much larger brightness of the agglomerate. (d) Corresponding trajectories of 20-nm colloid and a particle agglomerate, initially separated by 3 μm. Blue circles and red triangles show the distance between 20-nm colloid and particle agglomerate with respect to their start positions. Black squares show the distance between the 20-nm colloid and particle agglomerate.

that the NLC-particles' dispersion is less stable in a confined space, such as a micrometer-thin glass cell. For example, individual colloids exist for a shorter time of up to 4–6 h in the cell with thickness > 3 μm. The experiments therefore show that stability of the 20-nm colloids in dispersion is strongly affected by the thickness of the NLC cell. Furthermore, in our experiments in wedge cells, no suspended nanoparticles were observed in the part where thickness does not exceed

1–2.5 μm, and all colloids are anchored to the cell's surface during the filling process. The imperfections on the polyimide surface, such as those created during the polyimide rubbing process, are a strong source of nanoparticles' attraction. In contrast, individual nanoparticles were observed to migrate freely over all volume in a somewhat thicker, 3–6 μm cell.

Now, we have observed that 20-nm silica nanoparticles scarcely form stable aggregates in the NLC and, on the other hand, we notice that all single particles disappear from the NLC dispersion within 4–6 h after the cell was filled. This leads to the conjecture that the majority of the particles have been expelled to the surfaces of the cell, where they accumulate permanently.

Figure 5(a) shows a characteristic set of consecutive images of a 20-nm particle, which is trapped by the surface defect, whereas Fig. 5(a) shows the corresponding trajectory. The initial position of the particle is located at a distance of $\sim$2.5–3 μm from the surface defect. After $\sim$40 s of random motion, the particle starts moving towards the surface defect. After $\sim$90 s it anchors to the surface and fluctuates around the attraction point. The amplitude of fluctuations is in the range of $\pm$0.5 μm.

Another process, which is very efficient in immobilizing the nanoparticles and destabilizes the dispersion, is attraction of the single colloids to agglomerates of nanoparticles, remaining in the NLC. Unfortunately, not all clusters are split into individual colloids after sonification, and some aggregates are always present in the as-prepared dispersion. These residues may cause correspondingly large elastic distortions in the NLC and attract smaller particles. In Fig. 5(c) one can see a set of images showing the trapping and immobilization of a 20-nm colloidal particle by a larger aggregate. The trajectories of the colloid and the aggregate are shown in Fig. 5(d). The distance between the particle and aggregate is marked with the black line. After starting from about 3.5 μm, the separation between the nanoparticle and aggregate decreases and in $\sim$90 s colloids build a stable cluster.

IV. CONCLUSION

We have shown that the stability of dispersion of 20-nm colloidal particles in the nematic LC is a result of the balance between multiple phenomena. We observed that direct pair interaction of 20-nm homeotropic particles is very weak and does not result in significant agglomeration in diluted dispersions. For such a small particle size the attraction energy becomes comparable or lower than the thermal one. In addition to that, the particles are electrically charged and subjected to the electrostatic repulsion at separations smaller than the Debye screening length. The electric field of this surface charge also enhances the surface anchoring, and results in the larger distortions around 20-nm colloids, which might also influence the interparticle attraction. However, the low value of the estimated interaction potential (within 10 k_BT) does not allow one to eliminate the influences of the other possible mechanisms.

Our results show that in order to improve the colloidal stability of the NLC nanocolloidal dispersion in a confined environment, one should implement the process of removing larger clusters of nanoparticles by filtering procedure. Most importantly, one should use relatively large cell thickness in order to reduce surface trapping of nanoparticles and to secure enough free volume for the nanocolloids migration. The stability of NLC dispersions of nanoparticles in thin cells could be improved by using defect-free confining surfaces, with built-in electrostatic or chemical repulsion of nanoparticles.

ACKNOWLEDGMENTS

This work was supported by the European Commission Marie Curie project HIERARCHY Grant No. PITN-GA-2008-215851 (A.V.R.) and the Slovenian Research Agency (ARRS) Contracts No. P1-0099, No. J1-3612, and No. J1-6723. The authors thank M. Ravnik and S. Žumer for fruitful discussions. A.V.R. acknowledges Ivan Kvasič for assisting in the setup assembly.

[1] I. Ota, J. Ohnishi, and M. Yoshiyama, Proc. IEEE **61**, 832 (1973).
[2] B. Comiskey, J. D. Albert, H. Yoshizawa, and J. Jacobson, Nature (London) **394**, 253 (1998).
[3] E. A. Nance, G. F. Woodworth, K. A. Sailor, T.-Y. Shih, Q. Xu, G. Swaminathan, D. Xiang, C. Eberhart, and J. Hanes, Sci. Transl. Med. **4**, 149 (2012).
[4] Z. Wang and J. Zhe, Lab Chip **11**, 1280 (2011).
[5] Y. Kim, A. A. Shah, and M. J. Solomon, Nat. Commun. **5**, 3676 (2014).
[6] K. P. Velikov, C. G. Christova, R. P. A. Dullens, and A. van Blaaderen, Science **296**, 106 (2002).
[7] I. Muševič, M. Škarabot, U. Tkalec, M. Ravnik, and S. Žumer, Science **313**, 954 (2006).
[8] A. Nych, U. Ognysta, M. Škarabot, M. Ravnik, S. Žumer, and I. Muševič, Nat. Commun. **4**, 1489 (2013).
[9] C. Wu, A. B. Khanikaev, R. Adato, N. Arju, A. A. Yanik, H. Altug, and G. Shvets, Nat. Mater. **11**, 69 (2012).
[10] A. Moreau, C. Cirac, J. J. Mock, R. T. Hill, Q. Wang, B. J. Wiley, A. Chilkoti, and D. R. Smith, Nature (London) **492**, 86 (2012).
[11] J. A. Fan, C. Wu, K. Bao, J. Bao, R. Bardhan, N. J. Halas, V. N. Manoharan, P. Nordlander, G. Shvets, and F. Capasso, Science **328**, 1135 (2010).
[12] M. Petrov, B. Katranchev, P. M. Rafailov, H. Naradikian, U. Dettlaff-Weglikowska, E. Keskinova, and T. Spassov, Phys. Rev. E **88**, 042503 (2013).
[13] O. V. Yaroshchuk, L. O. Dolgov, and A. D. Kiselev, Phys. Rev. E **72**, 051715 (2005).
[14] S. Krishna Prasad, K. L. Sandhya, G. G. Nair, U. S. Hiremath, C. V. Yelamaggad, and S. Sampath, Liq. Cryst. **33**, 1121 (2006).
[15] A. Chaudhary, P. Malik, R. Mehra, and K. K. Raina, Phase Transit. **85**, 244 (2012).
[16] F. V. Podgornov, A. V. Ryzhkova, and W. Haase, Appl. Phys. Lett. **97**, 212903 (2010).
[17] H. Yoshida, Y. Tanaka, K. Kawamoto, H. Kubo, T. Tsuda, A. Fujii, S. Kuwabata, H. Kikuchi, and M. Ozaki, Appl. Phys. Express **2**, 121501 (2009).
[18] M. Trček, G. Cordoyiannis, V. Tzitzios, S. Kralj, G. Nounesis, I. Lelidis, and Z. Kutnjak, Phys. Rev. E **90**, 032501 (2014).

[19] S. Khatua, W.-S. Chang, P. Swanglap, J. Olson, and S. Link, Nano Lett. **11**, 3797 (2011).
[20] X. Chen, L. Chen, and Y. Chen, RSC Adv. **4**, 3627 (2014).
[21] B. Senyuk, J. S. Evans, P. J. Ackerman, T. Lee, P. Manna, L. Vigderman, E. R. Zubarev, J. van de Lagemaat, and I. I. Smalyukh, Nano Lett. **12**, 955 (2012).
[22] P. Poulin, H. Stark, T. C. Lubensky, and D. A. Weitz, Science **275**, 1770 (1997).
[23] H. Stark, Phys. Rep. **351**, 387 (2001).
[24] E. M. Terentjev, Phys. Rev. E **51**, 1330 (1995).
[25] R. W. Ruhwandl and E. M. Terentjev, Phys. Rev. E **55**, 2958 (1997).
[26] R. W. Ruhwandl and E. M. Terentjev, Phys. Rev. E **56**, 5561 (1997).
[27] V. S. R. Jampani, M. Škarabot, M. Ravnik, S. Čopar, S. Žumer, and I. Muševič, Phys. Rev. E **84**, 031703 (2011).
[28] M. Škarabot, M. Ravnik, S. Žumer, U. Tkalec, I. Poberaj, D. Babič, and I. Muševič, Phys. Rev. E **77**, 061706 (2008).
[29] I. Muševič, M. Škarabot, and M. Humar, J. Phys.: Condens. Matter **23**, 284112 (2011).
[30] M. Humar and I. Muševič, Opt. Express **18**, 26995 (2010).
[31] U. M. Ognysta, A. B. Nych, V. A. Uzunova, V. M. Pergamenschik, V. G. Nazarenko, M. Škarabot, and I. Muševič, Phys. Rev. E **83**, 041709 (2011).
[32] G. M. Koenig, Jr., J. J. de Pablo, and N. L. Abbott, Langmuir **25**, 13318 (2009).
[33] C. P. Lapointe, T. G. Mason, and I. I. Smalyukh, Science **326**, 1083 (2009).
[34] M. Škarabot and I. Muševič, Soft Matter **6**, 5476 (2010).
[35] A. V. Ryzhkova and I. Muševič, Phys. Rev. E **87**, 032501 (2013).
[36] B. Senyuk, D. Glugla, and I. I. Smalyukh, Phys. Rev. E **88**, 062507 (2013).
[37] Y. H. Fu, A. I. Kuznetsov, A. E. Miroshnichenko, Y. F. Yu, and B. Lukyanchuk, Nat. Commun. **4**, 1527 (2013).
[38] M. Škarabot, Ž. Lokar, and I. Muševič, Phys. Rev. E **87**, 062501 (2013).
[39] K. Kočevar and I. Muševič, Liq. Cryst. **28**, 599 (2001).
[40] J. Baumgartl, J. L. Arauz-Lara, and C. Bechinger, Soft Mater **2**, 631 (2006).
[41] M. B. McBride, Clays Clay Miner. **45**, 598 (1997).
[42] K. Kočevar and I. Muševič, Phys. Rev. E **65**, 030703(R) (2002).
[43] M. Škarabot and I. Muševič, J. Appl. Phys. **105**, 014905 (2009).
[44] A. Sawada, A. Manabe, and S. Naemura, Jpn. J. Appl. Phys. **40**, 220 (2001).
[45] A. V. Ryzhkova, F. V. Podgornov, A. Gaebler, R. Jakoby, and W. Haase, J. Appl. Phys. **113**, 244902 (2013).
[46] A. V. Ryzhkova, F. V. Podgornov, and W. Haase, Appl. Phys. Lett. **96**, 151901 (2010).
[47] O. D. Lavrentovich, I. Lazo, and O. P. Pishnyak, Nature (London) **467**, 947 (2010).
[48] O. D. Lavrentovich, Soft Matter **10**, 1264 (2014).
[49] A. K. Srivastava, A. C. Pandey, R. Kripal, and S. H. Lee, J. Mater. Sci. **49**, 1695 (2014).
[50] K. Tojo, A. Furukawa, T. Araki, and A. Onuki, Eur. Phys. J. E **30**, 55 (2009).